High-Overtone Thin Film Ferroelectric AlScN-on-Silicon Composite Resonators

Mingyo Park, Jialin Wang, Student Member, IEEE, *Azadeh Ansari, Member, IEEE*

***Abstract*— This letter presents the first demonstration of thin-film ferroelectric Aluminum Scandium Nitride (AlScN)-on-silicon composite resonators, targeting high-overtone resonance modes in the sub-6GHz band with a high figure of merit (FoM). The resonators are based on sputtered ferroelectric AlScN films with Sc/(Al+Sc) ratio of ~30% and thickness of ~1μm.**

Two types of AlScN thickness-extensional (TE) resonators are co-fabricated on the same SOI platform; with and without a 3.55μm-thick Si layer in the resonant stack. We show that although the passive Si device layer underneath the thin piezo-stack results in degradation of the electromechanical coupling coefficient (k_t^2), it boosts the quality factor (Q), provides structural robustness, and improves the overall $Q\times k_t^2$ FoM. The resonant frequency spectrum of the high-overtone TE modes of AlScN-on-Si composite resonator is analyzed and the dependency of k_t^2 on the Si device layer properties is studied. A high k_t^2 value of 11.7% at the 3rd-order TE resonant frequency of 2.4 GHz is reported, yielding a high $k_t^2\times Q_{max}$ FoM of 84. The reported FoM shows 2× improvement compared to the co-fabricated AlScN-only FBARs.

***Index Terms*— Composite FBAR (C-FBAR); Aluminum Scandium Nitride; ferroelectric; resonator.**

I. INTRODUCTION

EMERGING next generation wireless communication systems (4G LTE/5G) require extended frequency bands, larger bandwidths, and higher power handling capabilities while minimizing the complexity of filter architectures to fulfill the increased frequency spectrum utilization [1]–[4]. Thin-film bulk acoustic resonators (FBARs) have proven to be promising candidates for high-performance acoustic filters in 5G mid-band [2], [3]. Adding switching and tuning capability to the FBARs can reduce the overall filter size, complexity, and fabrication cost [5]. Recently, we reported on the frequency tuning and intrinsic polarization switching of FBARs based on ferroelectric $Al_{0.7}Sc_{0.3}N$ thin films [6], [7]. One of the challenges associated with the realization of polarization switching in acoustic resonators is the high voltages required for ferroelectric switching due to the ultra-wide bandgap of AlN [6]–[8]. Thus, piezo-stack thickness reduction (i.e. < few hundreds nm) is necessary to achieve lower coercive voltages.

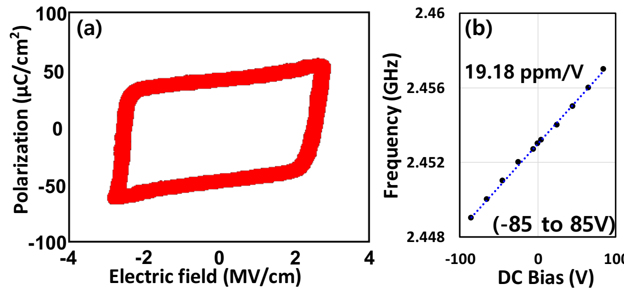

Fig. 1. (a) The hysteresis P-E loop of the $Al_{0.7}Sc_{0.3}N$ on Si C-FBAR with an area of 2.69×10^{-4}cm^2 and taken at an input frequency of 1kHz.(b) Frequency vs. DC voltage plot of f_3 mode C-FBAR with bias -85-85V.

Additionally, thinning down the film thickness is critical for scaling up the frequency of acoustic devices [9], [10]. However, the thickness reduction can pose fabrication challenges (*e.g.* high thin-film stress, low device yield), as well as increased self-heating, lower quality factor (Q), and unwanted nonlinearities. Such challenges make ultrathin acoustic resonators not desirable, particularly for high-power applications [11]–[15].

In this work, we demonstrate composite FBARs (C-FBARs), based on a thin-film $Al_{1-x}Sc_xN$ on Si, taking advantage of the enhanced electromechanical coupling coefficient (k_t^2) by using x= %30 [16]–[20]. A box-like ferroelectric hysteresis behavior is observed in C-FBARs with a coercive electric field at ~3 MV/cm and a linear frequency change is induced with bias voltage at -85V to 85V (Fig. 1). We demonstrate a high $k_t^2\times Q$ FoM, as a proof of concept and pathway for further thinning of the ferroelectric films deposited on the high-Q substrates. Adding a high-Q device layer underneath the sandwiched piezoelectric structure enables 1) high-frequency operation while maintaining the Q [21]–[23], 2) multi-mode resonance with mechanical robustness, avoiding thin-film stress issues found in conventional FBARs [24], and 3) higher power handling capability and lower self-heating due to including the substrate layer in the resonant stack [22], [25], [26].

The influence of the substrate in composite resonators is discussed in [21], [24], [27], [28]. Here, we demonstrate that C-FBARs show improved $k_t^2\times Q$ FoM, with a higher Q and lower k_t^2 compared to the co-fabricated FBARs. Furthermore, we provide design guidelines to optimize the passive substrate layer material and thickness, targeting the highest achievable

Manuscript received on November XX, 2020. This work was supported in part by the National Science Foundation under Grant ECCS-1542174 and in part by the National Science Foundation CAREER Award under Grant ECCS-1944304. (Corresponding author: Mingyo Park)

M. Park, J. Wang and, A. Ansari are with the School of Electrical and Computer Engineering, Georgia Institute of Technology, Atlanta, GA 30308 USA (e-mail: m.park@gatech.edu).

This article has been accepted for publication in a future issue of this journal, but has not been fully edited. Content may change prior to final publication. Citation information: DOI 10.1109/LED.2021.3070274, IEEE Electron Device Letters

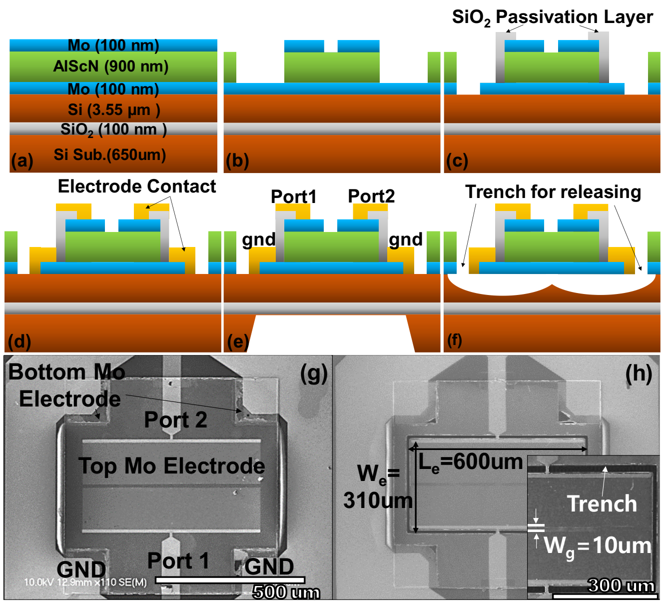

Fig. 2. The fabrication process of the AlScN C-FBARs and FBARs: (a) starting wafer cross-section schematic; (b) top electrode patterning and $Al_{0.7}Sc_{0.3}N$ etching; (c) bottom electrode patterning and SiO_2 isolation layer deposition; (d) Ti/Au deposition; (e) backside DRIE of Si handle layer to release C-FBARs; (f) front side release of the FBARs from Si device layer. The SEM images of (g) C-FBAR and (h) FBAR.

k_t^2. We analyze the dependency of k_t^2, the multi-mode resonant frequencies (f_r), and the spacing between two adjacent resonance modes (Δf) on the acoustic impedance ratio of the substrates to the piezo-film (Z_{sb}/Z_p) [27], [29]. We report on high-overtone ferroelectric AlScN-on-Si C-FBAR with Q_{max} of 720 and $k_t^2 \times Q_{max}$ FoM of 84, which is 2 times larger than the FoM of the co-fabricated AlScN-only FBAR.

II. Fabrication Process

The sequential fabrication process steps are demonstrated in Fig. 2. The 8-inch wafer consists of Mo/$Al_{0.7}Sc_{0.3}N$/Mo/Si/SiO_2 with the respective thicknesses of 0.1/0.9/0.1/3.55/0.1 μm (Fig. 2(a)). The piezo-stack is sputter-deposited on an SOI substrate using Von Ardenne CS 730S cluster at VTT Technical Research Center of Finland. The top/bottom Mo electrodes are etched using RIE with SF_4-based etchants. The $Al_{0.7}Sc_{0.3}N$ layer is etched using ICP with Cl_2-based etchants (Fig. 2(b)). A 150nm-thick SiO_2 passivation layer is deposited between top/bottom Mo layers for isolation (Fig. 2(c)). Ti/Au (15/300nm) layer is deposited as the contact pads (Fig. 2(d)). Finally, C-FBAR devices are released by DRIE from the wafer backside, leaving the 3.55 μm-thick Si device layer in a resonant stack (Fig. 2(e)). Mo/AlScN/Mo FBARs are released from the front side using trenches with XeF_2-based isotropic Si etching (Fig. 2(f)). Fig. 2(g), (h) show the scanning electron microscope (SEM) images of fabricated 2-port C-FBAR and FBAR.

III. Device Characteristics

The acoustic device performance is simulated using COMSOL finite element analysis (FEA). Fig. 3(a) illustrates the schematics of the four-layered C-FBAR. Fig. 3 (b) shows the simulated frequency response (FR) of the C-FBAR and

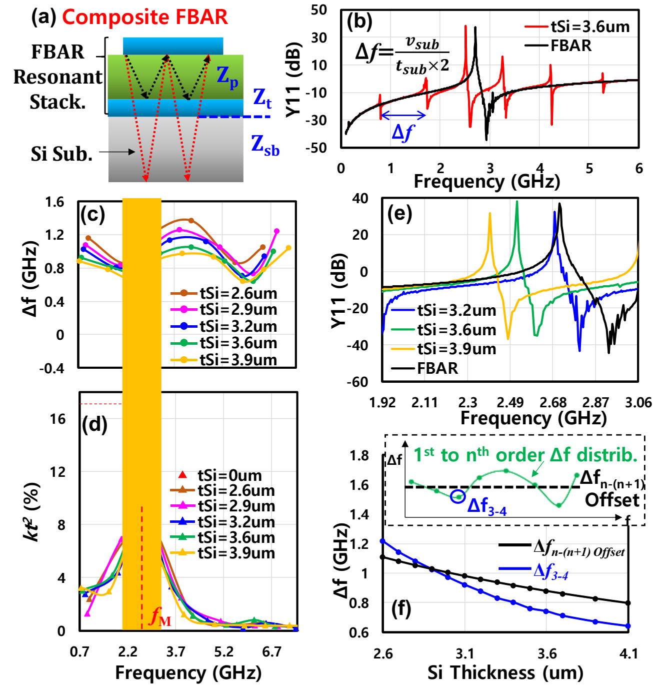

Fig. 3. (a) The schematic of the 4-layered C-FBAR. The FEA simulated results are analyzed; (b) The FR of Mo/AlScN/Mo FBAR and C-FBAR on Si substrate with Δf. The (c) Δf and (d) k_t^2 distributions of C-FBAR f_r(n) mode with varied tSi. (e) The FR of C-FBAR with varied tSi along with the FBAR. (f) The $\Delta f_{3\text{-}4}$ and offset $\Delta f_{n\text{-}(n+1)}$ *vs* tSi; the $\Delta f_{n\text{-}(n+1)}$ is evaluated using a pure Si with the same thickness of C-FBAR stack.

FBAR. The wideband FR of the FBAR shows a fundamental TE mode at the series/parallel resonant frequency (f_s/f_p) of 2.57/2.77GHz. The C-FBAR exhibits equidistant nth-order resonance (f_r(n)) modes with frequency spacing ($\Delta f_{3\text{-}4}$) of 0.74GHz between the f_r(3) and f_r(4).

The characteristics of the multiple resonance modes of C-FBARs are determined by the acoustic material properties and thicknesses of each layer. We analyze the distribution of $\Delta f_{n\text{-}(n+1)}$ and $k_t^2(n)$ to target the resonance mode with the highest FoM, beginning with the electrical input impedance (Z_{in}) of a four-layered C-FBAR [27], [29], [30]. The nth-order f_p(n)/f_s(n), can be extracted by setting $|Z_{in}| = \infty/0$. The distribution of k_t^2(n) and $\Delta f_{n\text{-}(n+1)}$ (i.e. Δf(n) between the adjacent f_p(n)/f_s(n) modes) can be calculated by [27], [29]:

$$k_t^2(n) = \frac{\pi^2}{4} \cdot \frac{f_s(n)}{f_p(n)} \cdot \left[1 - \frac{f_s(n)}{f_p(n)}\right]. \quad (1)$$

$$\Delta f_{s,p}(n) = f_{s,p}(n+1) - f_{s,p}(n). \quad (2)$$

It has been shown that the acoustic impedance ratio of the substrate to the piezoelectric film (Z_{sb}/Z_p) is critical in determining k_t^2(n), where two characteristic regions of Δf(n) exist: (i) normal (Δf_N, at $\gamma \approx n\pi$) and (ii) transition (Δf_T, at $\gamma \approx (n+1/2)\pi$) regions [27], [29]. When $Z_{sb}/Z_p < 1$ (*i.e.* soft substrate), maximum(max) k_t^2(n) is located at the first normal region ($\gamma \approx \pi$), which is close to $f = v/2t_p$. In other words, k_t^2(n) is max at the half-wavelength f_r of the piezoelectric film while Δf(n) carries the first minimum(min) value. Whereas when $Z_{sb}/Z_p > 1$ (*i.e.* hard substrate), max k_t^2 occurs at the first transition region ($\gamma \approx (1/2)\pi$), which is close to $f = v/4t_p$. In other words, k_t^2(n) is max at the quarter wavelength f_r of the piezoelectric film as Δf(n) has the first min value [27], [29].

This article has been accepted for publication in a future issue of this journal, but has not been fully edited. Content may change prior to final publication. Citation information: DOI 10.1109/LED.2021.3070274, IEEE Electron Device Letters

Here, the impact of the Si thickness on $k_t^2(n)$ and $\Delta f(n)$ is studied and illustrated in Fig. 3(c-d). The highest k_t^2 can be achieved from the $f_r(3)$ mode of C-FBAR with 3.2μm Si thickness when f_r of the C-FBAR matches the fundamental TE mode f_r of the FBAR (Fig.3(e)). In this work, since Z_{Si}/Z_{AlScN} <1, max k_t^2 is achieved when the $f_r(3)$ of C-FBAR matches f_M which is the half-wavelength f_r of the piezoelectric film (Fig. 3(d)).

Moreover, it is found that there is a strong correlation between the distribution of k_t^2 and Δf versus Si device layer thickness. Δf can be calculated based on the substrate acoustic phase velocity (v_{sb}) and thickness (t_{sb}) [25], [32], showing the adjustability of Δf by varying t_{sb} (Fig. 3(f)). $\Delta f_{n\text{-}(n+1)}$ with varied t_{sb} is plotted in Fig.3(c), presenting a periodic distribution vs. frequency. The observed ripples are caused by an acoustic impedance mismatch between Z_t and Z_{sb} from the multi-layer heterostructure [31]. It is observed that the f_r corresponding to the first min of $\Delta f(n)$ matches the fundamental TE f_r of FBAR. The max k_t^2 of C-FBAR can be obtained at the first normal region(Δf_N), which is close to the fundamental TE f_r of FBAR. Such characteristics offer design guidance to optimize the resonant stack critical to maximizing k_t^2.

IV. Experimental Results

Fig. 4 illustrates the measured and FEA-simulated wide-band FR of the FBAR and C-FBAR. Table I summarizes the characteristic of the measured nth-order resonance modes. The highest k_t^2 is achieved from 3rd-order TE mode with a resonance frequency closest to the fundamental TE f_r of AlScN-only FBAR. Fig. 5(a) demonstrates the corresponding zoomed-in peaks of the de-embedded Y_{11} magnitude and S_{11} phase of the $f_r(3)$ TE mode along with the Modified Butterworth Van Dyke (MBVD) model (Fig. 5(b)). The k_t^2 is extracted using f_s and f_p from the measured Y_{11} parameter (Fig. 5(c)) [10]. The unloaded quality factor (Q_m) of the resonator is estimated both from the Bode Q (Q_{Bode}) with S_{11} group delay, as well as the phase slope from the impedance Z_{11} parameter, where $\emptyset$ is the phase [33]:

$$Q_{Bode} = \omega \times \frac{|S_{11}|group\_delay(S_{11})}{1-|S_{11}|^2}, \quad (3)$$

$$Q_{s,p} = \frac{f_{s,p}}{2}\left|\frac{d\emptyset}{df}\right|. \quad (4)$$

TABLE I
CHARACTERISTICS OF MEASURED NTH-ORDER TE MODES IN C-FBAR

Mode	f_s (GHz)	f_s (GHz)	k_t^2(%)	$Q_{,max}$	$Q_{,max} \times k_t^2$
1	0.755	0.758	1.1	1038	11.42
2	1.619	1.644	3.69	369	13.62
3	2.348	2.471	11.69	720	84.16
4	3.023	3.117	7.2	550	39.65
5	3.859	3.959	6.06	533	32.34

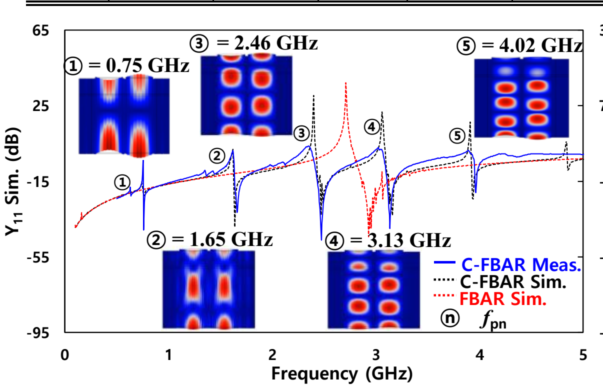

Fig. 4. Wideband Y_{11} FR of the measured (blue solid line) and simulated (black dotted line) C-FBAR, along with the simulated FBAR (red dotted line). 2D cross-section displacements of nth-order TE mode are shown.

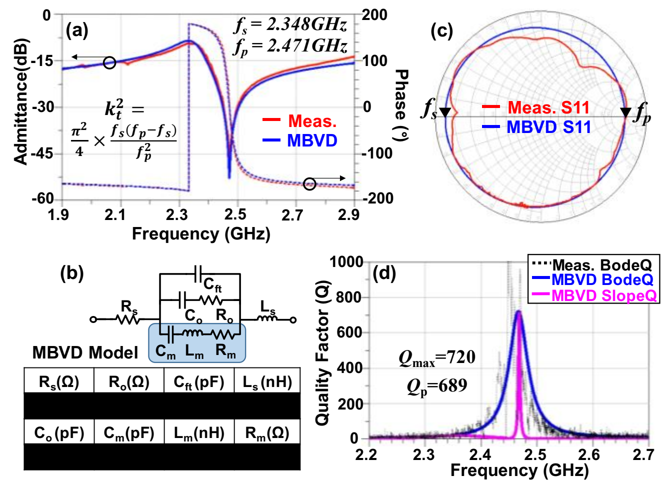

Fig. 5. Measured and MBVD-fitted results of AlScN-on-Si C-FBAR. (a)–(b) Zoomed-in C-FBAR admittance and S11 phase plot along with Modified Butterworth-Van Dyke (MBVD) fitted model, (c)-(d): Smith chart demonstration of S_{11} and computed C-FBAR Bode Q.

Fig. 5(c) illustrates the measured S_{11} parameter fitted with the MBVD model of the continuous Q circle. The Q circle is placed at the center of the Smith chart by using source impedance matching. The Q_{Bode} versus frequency (3) and $Q_{s,p}$ versus frequency (4) are plotted in Fig. 5(d). The computed Q_p of 689 and Q_{max} of 720 are obtained from the MBVD-fitted model. The relatively low Q_s are attributed to the large ohmic losses in R_s. Future work will focus on improving Q_s with bordering to suppress spurious modes and optimizing metal electrodes to reduce ohmic losses [34], [35].

V. Conclusion

We reported on ferroelectric AlScN FBARs and AlScN-on-Si high-overtone composite FBARs, fabricated on the same SOI platform. The measurement results of $Al_{0.7}Sc_{0.3}N$ FBAR and C-FBAR are compared in Table II. By including a 3.55μm-thick Si substrate underneath the piezo-stack, an FoM ($Q_p \times k_t^2$) of 80 was achieved, which is 2 times larger than AlScN FBAR FoM [6], [7]. This work provides a single-chip multi-frequency solution for RF filters in the sub-6GHz band with a high FoM.

TABLE II
$AL_{1-X}SC_XN$ BASED TE MODE ACOUSTIC RESONATOR FOM COMPARISON

	*On Sub**	Sc_x (%)	f_p (GHz)	Q_p	k_t^2(%)	$Q_p \times k_t^2$
SMR[19]	Y	20	2.4	650	12.3	79.95
XBAW[20]	N	28	3.4	831	14.82	123.1
FBAR[14]	N	9	2.23	513	9.5	48.73
FBAR [6]	N	28	3.17	210	18.1	38
C-FBAR[28]	Y	0	3.26	2507**	2.12	53.1
This Work	Y	28	2.47	689	11.7	80.54

*: Piezo-on-substrate; **: Q_{max} from MBVD

References

[1] J. B. Shealy, R. Ventury, S. R. Gibb, M. D. Hodge, P. Patel, M. A. Mclain, A. Y. Feldman, M. D. Boomgarden, M. P. Lewis, B. Hosse, and R. Holden, "Low loss, 3.7GHz wideband BAW filters, using high power single crystal AlN-on-SiC resonators," *IEEE MTT-S Int. Microw. Symp. Dig.*, pp. 1476–1479, 2017, doi: 10.1109/MWSYM.2017.8058901.

[2] D. Moy, "Avago Technologies ' FBAR Filter Technology Designed Into Latest Generation of 4G & LTE Smartphones White Paper," *Avago Technologies*, 2012. www.avagotech.com.

[3] Qorvo, "A New Generation of 5G Filter Technology," *Qorvo*, 2020. www.qorvo.com.

[4] R. Ruby, "A Snapshot in Time: The Future in Filters for Cell Phones," *IEEE Microw. Mag.*, vol. 16, no. 7, pp. 46–59, Aug. 2015, doi: 10.1109/MMM.2015.2429513.

[5] S. S. Gevorgian, A. k. Tagantsev, and A. K. Vorobiev, "Introduction," in *Tuneable Film Bulk Acoustic Wave Resonators*, London, U.K.: Springer, 2013, pp. 1–15.

[6] J. Wang, M. Park, S. Mertin, T. Pensala, F. Ayazi, and A. Ansari, "A Film Bulk Acoustic Resonator Based on Ferroelectric Aluminum Scandium Nitride Films," *J. Microelectromechanical Syst.*, vol. 29, no. 5, pp. 741–747, Oct. 2020, doi: 10.1109/JMEMS.2020.3014584.

[7] J. Wang, M. Park, S. Mertin, T. Pensala, F. Ayazi, and A. Ansari, "A High-kt2 Switchable Ferroelectric Al0.7Sc0.3N Film Bulk Acoustic Resonator," 2020.

[8] E. Defaÿ N. Ben Hass ine, P. Emery, G. Parat, J. Abergel, and A. Devos, "Tunability of aluminum nitride acoustic resonators: A phenomenological approach," *IEEE Trans. Ultrason. Ferroelectr. Freq. Control*, vol. 58, no. 12, pp. 2516–2520, 2011, doi: 10.1109/TUFFC.2011.2114.

[9] M. Ueda, M. Hara, S. Taniguchi, T. Yokoyama, T. Nishihara, K. Hashimoto, and Y. Satoh, "Development of an X-band filter using air-gap-type film bulk acoustic resonators," *Jpn. J. Appl. Phys.*, vol. 47, no. 5 PART 2, pp. 4007–4010, 2008, doi: 10.1143/JJAP.47.4007.

[10] M. Park, J. Wang, R. Dargis, A. Clark, and A. Ansari, "Super High-Frequency Scandium Aluminum Nitride Crystalline Film Bulk Acoustic Resonators," in *2019 IEEE International Ultrasonics Symposium (IUS)*, Oct. 2019, pp. 1689–1692, doi: 10.1109/ULTSYM.2019.8925598.

[11] F. Martin, P. Muralt, M.-A. Dubois, and A. Pezous, "Thickness dependence of the properties of highly *c* -axis textured AlN thin films," *J. Vac. Sci. Technol. A Vacuum, Surfaces, Film.*, vol. 22, no. 2, pp. 361–365, 2004, doi: 10.1116/1.1649343.

[12] A. Iqbal and F. Mohd-Yasin, "Reactive sputtering of aluminum nitride (002) thin films for piezoelectric applications: A review," *Sensors (Switzerland)*, vol. 18, no. 6, pp. 1–21, 2018, doi: 10.3390/s18061797.

[13] F. Z. Bi and B. P. Barber, "Bulk acoustic wave RF technology," *IEEE Microw. Mag.*, vol. 9, no. 5, pp. 65–80, 2008, doi: 10.1109/MMM.2008.927633.

[14] M. D. Hodge and J. B. Shealy, "High Power , Wideband Single Crystal XBAW Technology for sub-6 GHz Micro RF Filter Applications," *IEEE Int. Ultrason. Symp.*, pp. 6–9, 2018, doi: 10.1109/ULTSYM.2018.8580045.

[15] T. Yokoyama, M. Rara, M. Veda, and Y. Satoh, "K-band ladder filters employing air-gap type thin film bulk acoustic resonators," *Proc. - IEEE Ultrason. Symp.*, pp. 598–601, 2008, doi: 10.1109/ULTSYM.2008.0143.

[16] K. Umeda, H. Kawai, A. Honda, M. Akiyama, T. Kato, and T. Fukura, "Piezoelectric properties of ScAlN thin films for piezo-MEMS devices," *Proc. IEEE Int. Conf. Micro Electro Mech. Syst.*, pp. 733–736, 2013, doi: 10.1109/MEMSYS.2013.6474347.

[17] M. Moreira, J. Bjurström, I. Katardjev, and V. Yantchev, "Aluminum scandium nitride thin-film bulk acoustic resonators for wide band applications," *Vacuum*, vol. 86, no. 1, pp. 23–26, 2011, doi: 10.1016/j.vacuum.2011.03.026.

[18] M. Park, Z. Hao, R. Dargis, A. Clark, and A. Ansari, "Epitaxial Aluminum Scandium Nitride Super High Frequency Acoustic Resonators," *J. Microelectromechanical Syst.*, vol. 29, no. 4, pp. 490–498, Aug. 2020, doi: 10.1109/JMEMS.2020.3001233.

[19] A. Bogner, R. Bauder, H. Timme, T. Forster, C. Reccius, R. Weigel, and A. M. Hagelauer, "Enhanced Piezoelectric AL1-XSCXN RF-MEMS Resonators for Sub-6 GHz RF-Filter Applications: Design, Fabrication and Characterization," *Proc. IEEE Int. Conf. Micro Electro Mech. Syst.*, vol. 2020-Janua, pp. 1258–1261, 2020, doi: 10.1109/MEMS46641.2020.9056296.

[20] C. Moe, R. H. Olsson III, P. Patel, Z. Tnag, M. D'Agati, M. Winters, R. Ventury, and J. Shealy, "Highly Doped AlScN 3.5 GHz XBAW Resonators with 16% k2eff for 5G RF Filter Applications," *Proc. 2020 IEEE Ultrason. Symp.*, pp. 1–4, 2020.

[21] H. Zhang, W. Pang, H. Yu, and E. S. Kim, "High-tone bulk acoustic resonators on sapphire, crystal quartz, fused silica, and silicon substrates," *J. Appl. Phys.*, vol. 99, no. 12, 2006, doi: 10.1063/1.2209029.

[22] R. Abdolvand and F. Ayazi, "7E-4 Enhanced Power Handling and Quality Factor in Thin-Film Piezoelectric-on-Substrate Resonators," in *2007 IEEE Ultrasonics Symposium Proceedings*, Oct. 2007, pp. 608–611, doi: 10.1109/ULTSYM.2007.158.

[23] G. K. Ho, R. Abdolvand, A. Sivapurapu, S. Humad, and F. Ayazi, "Piezoelectric-on-silicon lateral bulk acoustic wave micromechanical resonators," *J. Microelectromechanical Syst.*, vol. 17, no. 2, pp. 512–520, 2008, doi: 10.1109/JMEMS.2007.906758.

[24] T. A. Gosavi, E. R. MacQuarrie, G. D. Fuchs, and S. A. Bhave, "HBAR as a high frequency high stress generator," in *2015 IEEE International Ultrasonics Symposium*, 2015, pp. 24–27, doi: 10.1109/ULTSYM.2015.0361.

[25] T. Daugey, J. M. Friedt, G. Martin, and R. Boudot, "A high-overtone bulk acoustic wave resonator-oscillator-based 4.596 GHz frequency source: Application to a coherent population trapping Cs vapor cell atomic clock," *Rev. Sci. Instrum.*, vol. 86, no. 11, 2015, doi: 10.1063/1.4935172.

[26] S. Ballandras, T. Baron, E. Lebrasseur, G. Martin, D. Gachon, A. Reinhardt, P.-P. Lassagne, J.-M. Friedt, L. Chommeloux, and D. Rabus, "High overtone Bulk Acoustic Resonators : application to resonators , filters and sensors," *Acoustics*, 2012, doi: hal-00811239.

[27] M. Liu, J. Li, C. Wang, J. Li, and J. Ma, "Influence of electrodes on the effective electromechanical coupling coefficient distributions of high-overtone bulk acoustic resonator," *Ultrasonics*, vol. 56, pp. 566–574, 2015, doi: 10.1016/j.ultras.2014.10.014.

[28] G. Pillai, A. A. Zope, J. M. L. Tsai, and S. S. Li, "Design and Optimization of SHF Composite FBAR Resonators," *IEEE Trans. Ultrason. Ferroelectr. Freq. Control*, vol. 64, no. 12, pp. 1864–1873, 2017, doi: 10.1109/TUFFC.2017.2759811.

[29] Y. Zhang, Z. Wang, and J. D. N. Cheeke, "Resonant spectrum method to characterize piezoelectric films in composite resonators," *IEEE Trans. Ultrason. Ferroelectr. Freq. Control*, vol. 50, no. 3, pp. 321–333, 2003, doi: 10.1109/TUFFC.2003.1193626.

[30] K.-Y. Hashimoto, *RF Bulk Acoustic Wave Filters for Communications*. Artech House, 2009.

[31] V. J. Gokhale, B. P. Downey, D. S. Katzer, M. T. Hardy, N. Nepal, and D. J. Meyer, "Engineering Efficient Acoustic Power Transfer in HBARs and Other Composite Resonators," *J. Microelectromechanical Syst.*, pp. 1–6, 2020, doi: 10.1109/jmems.2020.3009516.

[32] V. J. Gokhale, B. P. Downey, D. S. Katzer, N Nepal, A. C. Lang, R. M. Stroud, and D. J. Meyer, "Epitaxial bulk acoustic wave resonators as highly coherent multi-phonon sources for quantum acoustodynamics," *Nat. Commun.*, vol. 11, no. 1, p. 2314, 2020, doi: 10.1038/s41467-020-15472-w.

[33] D. A. Feld, R. Parker, R. Ruby, P. Bradley, and S. Dong, "After 60 years: A new formula for computing quality factor is warranted," in *IEEE Ultrasonics Symposium*, 2008, no. 6, pp. 431–436, doi: 10.1109/ULTSYM.2008.0105.

[34] J. Kaitila, M. Ylilammi, J. Ellä, and R. Aigner, "Spurious resonance free bulk acoustic wave resonators," *Proc. IEEE Ultrason. Symp.*, vol. 1, no. IL, pp. 84–87, 2003, doi: 10.1109/ultsym.2003.1293361.

[35] R. Thalhammer, G. Fattinger, M. Handtmann, and S. Marksteiner, "Ohmic effects in BAW-resonators," *IEEE MTT-S Int. Microw. Symp. Dig.*, pp. 390–393, 2006, doi: 10.1109/MWSYM.2006.249552.